Tetrahedron 65 (2009) 1017–1025

Contents lists available at ScienceDirect

Tetrahedron

journal homepage: www.elsevier.com/locate/tet

Structure, bonding, and aggregation of selenium-containing organolithium species

Lawrence M. Pratt [a,*], Shin-ichi Fujiwara [b], Nobuaki Kambe [c]

[a] Department of Chemistry, Fisk University, 1000 17th Ave. N., Nashville, TN 37208, USA
[b] Department of Chemistry, Osaka Dental University, 8-1 Kuzuhahanazono-cho, Hirakata, Osaka 573-1121, Japan
[c] Department of Applied Chemistry, Graduate School of Engineering, Osaka University, 2-1 Yamadaoka, Hirakata, Osaka 573-1121, Japan

ARTICLE INFO

Article history:
Received 12 August 2008
Received in revised form 24 November 2008
Accepted 26 November 2008
Available online 30 November 2008

ABSTRACT

1,3-Dioxo compounds can be prepared from selenium-mediated carbonylation of lithium enolates in the presence of carbon monoxide. Intermediates in this reaction include several organic species that contain both selenium and lithium. The first step in understanding the detailed reaction mechanism is to understand the structure of these intermediates. Like most organolithium compounds, these species can exist as aggregates in solution. The B3LYP density functional theory (DFT) method was used to examine the gas phase and THF solvated structures of these compounds. The calculations showed that each of the compounds forms dimers or higher aggregates in the gas phase. Aggregates are also formed in THF solution, although solvation favors lower aggregates as compared to the gas phase.

1. Introduction

We have developed selenium-mediated carbonylation of organolithium compounds with carbon monoxide[1–3] leading to the corresponding selenol esters[4] after trapping with alkyl halides. We have also investigated related reactions.[5] Among them, lithium enolates of aldehydes and ketones can be carbonylated to afford β-formyl and β-keto selenol esters having 1,3-dioxoalkane units,[2a] which are frequently encountered frameworks of organic molecules as versatile and important functionalities in synthetic chemistry. As for the mechanism of this reaction, we proposed a unique carbonylation mechanism comprising O-carbonylation and subsequent migration of the SeCO moiety to the α-carbon as shown in Scheme 1. Reaction of enolates with Se affords selenolates **3**,[6] which then react with CO to give lithium selenocarbonates **4** as an initial carbonylation intermediate probably via formal rearrangement of **5**.[7–9] In the cases of enolates of aldehydes, selenocarbonates are obtained at −23 °C or below by alkylation of **4**, while **4** undergoes an apparent [1,3]-rearrangement at 0 °C or above to lithium selenocarboxylates **2** giving β-formyl selenol esters. However, none of the O-carbonylation products were obtained from enolates of ketones and other carbonyl compounds even at −23 °C. These results suggest that rearrangement from **4** to **2** is rapid when $R^1 \neq H$ probably due to steric repulsion between R^1 and OC(O)SeLi moiety.

The mechanism is likely to be much more complex due to the formation of aggregates of these species. The pioneering work of Brown and co-workers helped to establish that organolithium compounds generally exist as aggregates.[10,11] Aggregates of lithium enolates,[12–22] alkyllithiums,[23–26] lithium dialkyamides,[27–33] and other organolithium compounds[34–38] are well known, and often affect their reactivity and selectivity. This work has been extended to chiral systems, using chiral lithium dialkylamides and butyllithium mixed aggregates with chiral lithium dialkylamides for asymmetric reactions.[39,40] Therefore, knowledge of the possible aggregation states of the selenium-containing intermediates is an important step in determining the reaction mechanisms. The reactivity of any aggregate or monomer will depend on its mole fraction and on its activation energy. Thus, even a minor species can contribute to the reaction if it is more reactive than the other aggregates. In this paper we investigated the structure of lithium selenoacetate (**1**) as the simplest member of this family of compounds. We also investigated the structures of the proposed reactive intermediates (**2**–**5**), where $R_1{=}R_2{=}R_3{=}H$. It has already been established that most lithium enolates are hexamers in hydrocarbon solvents and tetramers in THF solution.[12] This was done by comparing the computational results with the experimental data. This comparison showed that although the B3LYP density functional method is imperfect, it generally predicts aggregation states that agree with the experimental data for this type of system. Enolate monomers and dimers may also exist in very dilute THF solutions.[13] The possibility of lithium chelation in the selenium-containing compounds **1**–**5** makes it unlikely that aggregates

* Corresponding author.
E-mail address: lpratt@fisk.edu (L.M. Pratt).

0040-4020/$ – see front matter © 2008 Elsevier Ltd. All rights reserved.
doi:10.1016/j.tet.2008.11.087

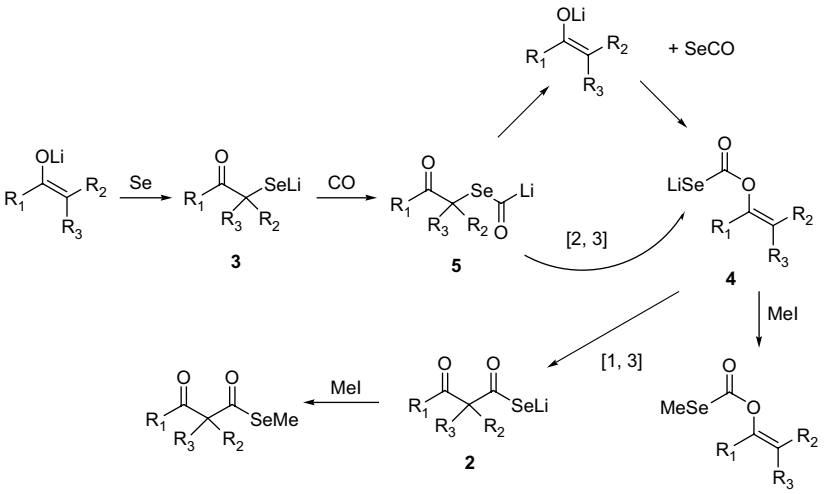

Scheme 1. Proposed reaction mechanism for selenium-mediated enolate carbonylation.

higher than a tetramer will be formed. We therefore examined the structures of the monomer, dimer, trimer, and tetramer.

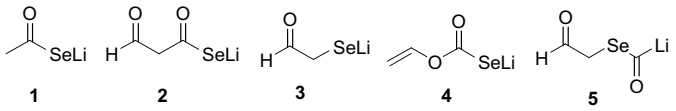

Density functional theory (DFT) calculations have successfully predicted the aggregation state of a number of organolithium compounds, including alkyllithiums, lithium dialkylamides, and lithium enolates.[12,26,33] The B3LYP functional with the 6-31+G(d) basis set was used for all geometry optimizations and frequency calculations. Because basis set superposition errors (BSSEs) can be significant with heavy atoms such as selenium, single point energy calculations were performed with the 6-311+G(2df,2pd) basis set.

2. Computational methods

All calculations were performed using *Gaussian 98* or *Gaussian 03*.[41] The objective is to calculate the standard free energy of a lithium selenoester solute, which is given by:

$$G_T^{\circ}(\text{solute}) \rightarrow G_T^{\circ}(\text{gas}) + \Delta G_S^{\circ} \tag{1}$$

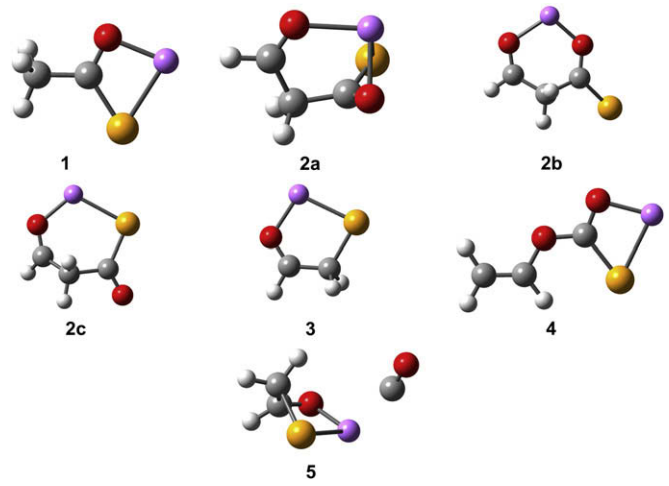

Figure 1. Optimized geometries of monomeric **1**–**5**. Gray: carbon; white: hydrogen; red: oxygen; yellow: selenium; violet: lithium.

where $G_T^{\circ}(\text{gas})$ is the standard gas-phase free energy at temperature T and ΔG_S° is the standard free energy of solvation. The micro-solvation model assumes that the latter is given by the free energy change when a gas-phase organolithium molecule $(\text{RCOSeLi})_n$ is coordinated to m explicit solvent ligands E (in this case THF):

$$(\text{RCOSeLi})_n + m\text{E} \rightarrow (\text{RCOSeLi})_n\text{E}_m. \tag{2}$$

In other words, the free energy of a gas-phase 'supermolecule' $(\text{RCOSeLi})_n\text{E}_m$ relative to that of $(\text{RCOSeLi})_n$ and m solvent molecules is assumed to yield the free energy of the solvated molecule $(\text{RCOSeLi})_n$ in the condensed phase. The gas-phase free energies of the relevant species are calculated by:

$$G_T^{\circ}(\text{gas}) = E_{\text{EN}} + E_0^{\text{vib}} + \Delta G_T^{\circ} \tag{3}$$

where the terms on the right hand side as well as the procedure used for calculating them are described below.

The geometry of each molecule was first optimized and the vibrational frequencies calculated at the B3LYP/6-31+G(d) level of theory, and single point energies were calculated with the 6-311+G(2df,2pd) basis set at the 6-31+G(d) geometries. Then the terms in Eq. 3 are:

E_{EN}=the electronic energy plus nuclear repulsion of the equilibrium geometry, using B3LYP/6-31+G(d) or B3LYP/6-311+G(2df,2pd).
E_0^{vib}=unscaled B3LYP/6-31+G(d) vibrational zero point energy.
ΔG_T°=B3LYP/6-31+G(d) thermal corrections to the free energy for a standard state of 1 atm and specified temperature. This includes contributions from translational, rotational, and vibrational degrees of freedom.
ΔG°=free energy changes for the 'reactions' (dimerizations, tetramerizations, mixed aggregate formation, etc.) obtained as the sum of the $G_T^{\circ}(\text{gas})$ values of products minus those for reactants.

It is necessary to convert the usual gas-phase standard free energies, which correspond to a standard state 1 atm to the

Table 1
Conformational free energies of gas-phase β-ketoselenocarboxylate (**2**)

Basis set	Temp (K)	**2a**	**2b**	**2c**
6-31+G(d)	200	0	1.24	3.29
6-311+(2df,2pd)	200	0	0.626	0.012
6-31+G(d)	298.15	0	1.04	2.96
6-311+(2df,2pd)	298.15	0	0.426	−0.322

Table 2
Calculated free energies of gas-phase dimer formation (kcal/mol per Li)

Molecule	Temp (K)	6-31+G(d)	6-311+G(2df,2pd)
1	200	−18.2	−12.5
2	200	−23.6	−21.7
3	200	−17.9	−11.9
4	200	−19.2	−13.5
1	298.15	−16.2	−10.5
2	298.15	−22.0	−20.0
3	298.15	−16.1	−10.1
4	298.15	−17.2	−11.5

Table 3
Calculated free energies of gas-phase *anti*-trimer formation (kcal/mol per Li)

Molecule	Temp (K)	6-31+G(d)	6-311+G(2df,2pd)
1	200	−4.60[a]	−2.50[a]
2	200	−4.64	−2.32
3	200	−5.66	−1.18
4	200	−6.49[a]	−2.68[a]
1	298.15	−3.84[a]	−1.74[a]
2	298.15	−4.12	−1.80
3	298.15	−5.01	−0.534
4	298.15	−5.68[a]	−1.88[a]

[a] Trimer was planar, no *anti*/*syn* conformers.

appropriate standard state for a solution, which is taken as 1 mol L^{-1}. The details of these conversions have been previously published.[42] These corrections amount to 1.11 kcal/mol at 200 K and 1.89 kcal/mol at 298 K. These conversion terms were included in all solution-phase reactions below.

Another conversion is required for proper treatment of the explicit solvent molecules used in microsolvation. The traditional approach is to set the standard state of a pure liquid to be the concentration of the pure liquid itself, which then allows one to drop the concentration of the pure liquid from equilibria expressions. In contrast, as an example, since we have decided to adopt the standard state of 1 mol L^{-1} for all species, the directly calculated free energy change for the process

$$2RCOSeLiE_2 \rightarrow (RCOSeLiE)_2 + 2E \quad (4)$$

contains the concentration of E and is given by:

$$\Delta G^{o} = -RT \ln \frac{[(RLiE)_2]}{[RLiE_2]^2} - 2RT \ln[E] \quad (5)$$

where all concentrations are evaluated at equilibrium (recall that E is THF). To evaluate the final term of Eq. 5, the molarity of THF solvent was calculated at each temperature from its tabulated density.[43] The corrections due to the second term in the equation above are equal to −1.03, and −1.49 kcal/mol per THF at 200 and 298 K, respectively. These corrections were added to the directly calculated free energy changes for the reactions in solution so that the standard free energy changes reported here correspond to the equilibrium constants as usually written, that is, without solvent concentrations. Thus, the $-2RT$ ln[THF] term in Eq. 5 will favor the disolvated monomer by 2.0546 kcal/mol at 200 K.

Table 4
Calculated free energies of gas-phase *syn*-trimer formation (kcal/mol per Li)

Molecule	Temp (K)	6-31+G(d)	6-311+G(2df,2pd)
1	200	N/A	N/A
2	200	−4.02	1.44
3	200	−5.55	−3.12
4	200	N/A	N/A
1	298.15	N/A	N/A
2	298.15	−3.30	2.17
3	298.15	−4.95	−2.52
4	298.15	N/A	N/A

In order to gain insight into the reaction mechanisms, activation barrier heights were calculated for two reactions of **5**. Transition structures were optimized at the B3LYP/6–31+G(d) level, followed by frequency calculation at the same level to obtain thermal corrections to the free energy. The transition structure geometries were re-optimized at the MP2/6-31+G(d) level. IRC calculations were also performed at the MP2/6-31+G(d) level to ensure that the correct transition structures connecting the reactants and products were found.

3. Results and discussion

Geometry optimizations were performed on lithium selenoacetate (**1**), lithium β-ketoselenocarboxylate (**2**), lithium α-ketoselenolate (**3**), lithium *O*-vinylselenocarbonate (**4**), and the carbonyl adduct of the lithium ketoselenolate (**5**). The gas-phase monomers, dimers, and tetramers were examined, and explicit THF ligands were used to model these structures in solution. The optimized geometries of the gas-phase monomers are shown in Figure 1.

The monomeric lithium β-ketoselenocarboxylate (**2**) can exist in three gas-phase conformations, shown in Figure 1, with the most stable conformation chelating the lithium atom by selenium and both oxygen atoms at 200 K. The relative energies of the three conformations are listed in Table 1. The relative energies of the conformers were nearly independent of temperature, but showed a significant dependence on the basis set.

Lithium ketoselenolate (**5**) did not optimize to a stable monomeric form. Instead, geometry optimization generated a dipole–dipole complex between (**3**) and CO, which was found to be a local minimum by the frequency calculation on the optimized geometry.

The free energies of gas-phase dimer, trimer, and tetramer formation were calculated according to Eqs. 6–8, respectively. The results are shown in Tables 2–4.

$$2monomer \rightarrow dimer \quad (6)$$

$$3/2dimer \rightarrow trimer \quad (7)$$

$$2dimer \rightarrow tetramer \quad (8)$$

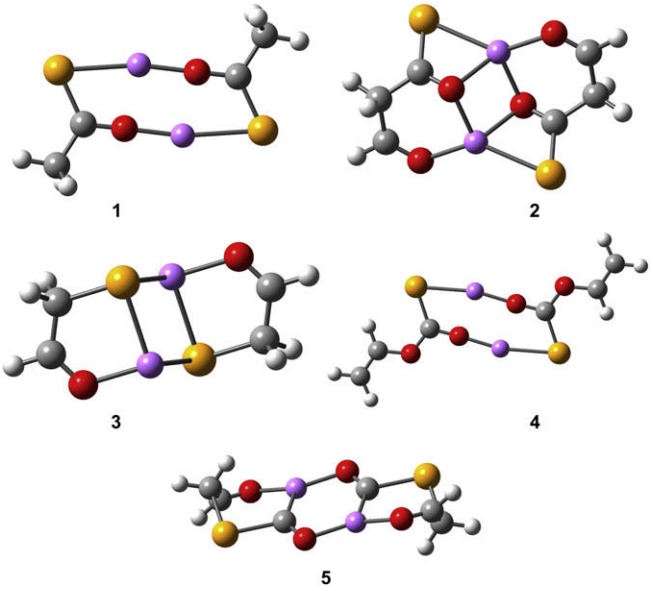

Figure 2. Optimized geometries of dimeric **1**–**5**.

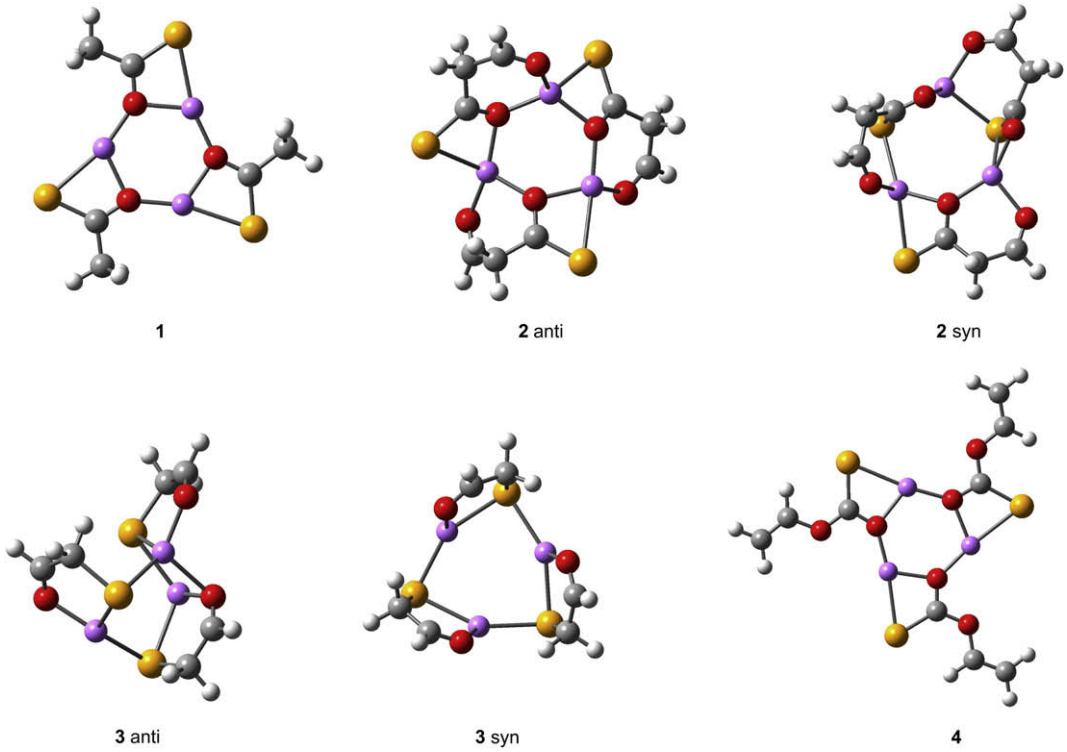

Figure 3. Optimized geometries of trimeric **1**–**4**.

Compounds **1**–**4** can dimerize with the lithium atoms coordinated to both oxygen and selenium in several possible structures, and the most stable structures are shown in Figure 2. The corresponding dimerization free energies are given in Table 2. The most exergonic dimerization free energy was found for lithium α-ketoselenolate (**2**), which was able to maximize the coordination sphere of lithium, with each lithium atom bonded to three oxygen atoms and one selenium atom. Lithium selenoacetate (**1**) and *O*-vinylselenocarbonate (**4**) optimized to planar geometries, while the extra one or two methylene groups in **2** and **3** allowed for a non-planar geometry with more chelation of the lithium atom. Unlike the monomer, aggregates of **5** optimized to a structure that is isomeric with **4**, with the dimer of **5** shown in Figure 2. Although the dimer, trimer, and tetramer of **5** were optimized to local minima in the gas phase, they were high energy species relative to **4**, and are not expected to be present in significant amounts. Aggregates of **5** are therefore not considered further in this work.

Similar types of lithium coordination were found for the trimers. Compounds **1** and **4** formed planar trimers, while the greater

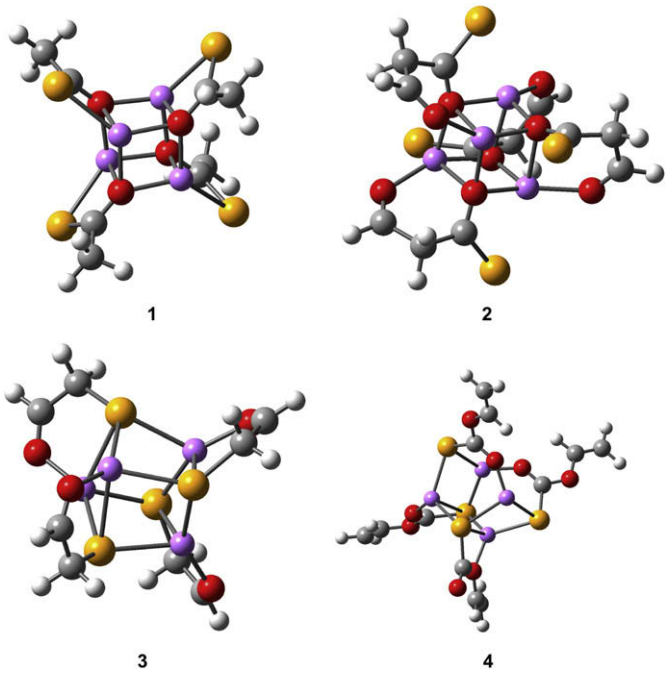

Figure 4. Optimized geometries of tetrameric **1**–**4**.

Table 5
Calculated free energies of gas-phase tetramer formation from the dimer (Eq. 8, kcal/mol per Li)

Molecule	Temp (K)	6-31+G(d)	6-311+G(2df,2pd)
1	200	−7.68	−3.82
2	200	−8.37	−1.61
3	200	−10.2	−3.09
4	200	−11.6	−3.46
1	298.15	−6.68	−2.83
2	298.15	−7.04	−0.274
3	298.15	−9.28	−2.15
4	298.15	−10.7	−2.56

Table 6
Calculated free energies of gas-phase tetramer formation from the most stable trimer (Eq. 9, kcal/mol per Li)

Molecule	Temp (K)	6-31+G(d)	6-311+G(2df,2pd)
1	200	−3.07	−1.32
2	200	−3.73	0.709
3	200	−4.66	0.0358
4	200	−5.06	−0.780
1	298.15	−2.84	−1.09
2	298.15	−2.91	1.53
3	298.15	−4.33	0.362
4	298.15	−4.97	−0.684

Table 7
Calculated third solvation free energy for compounds **1**–**4** at 200 K [298.15 K] (kcal/mol)

Molecule	6-31+G(d)	6-311+G(2df,2pd)
1	0.553 [2.73]	0.594 [2.77]
2	−0.144 [2.20]	1.52 [3.86]
3	0.435 [2.41]	6.66 [8.64]
4	−1.58 [0.534]	2.23 [4.34]

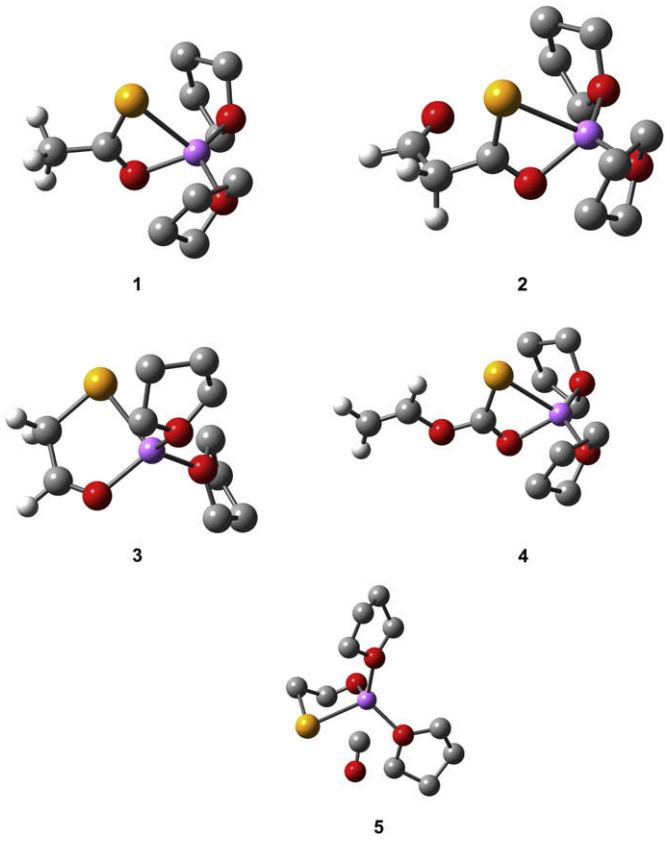

Figure 5. Optimized geometries of THF solvated monomers of compounds **1**–**5**.

flexibility of **2** and **3** allowed for non-planar structures, as shown in Figure 3. The latter two compounds optimized to two different trimers, the *syn*, with all three groups on the same side of the lithium-containing ring; and the *anti* isomer, with one group opposite to the other two. The corresponding free energies of trimer formation are shown in Tables 3 and 4. The trimeric form of **4** is more stable than the dimer, apparently because of improved chelation of the lithium atoms by the vinyloxide oxygen.

Figure 4 shows the optimized geometries of the gas-phase tetramers and the corresponding aggregation free energies are given in Table 5. In order to directly compare the stability of the trimers and tetramers, the free energies of tetramer formation from the trimer were calculated according to Eq. 9. Comparison of the energies in Tables 2–6 shows that compounds **1**–**4** exist largely as trimers and tetramers in the gas phase.

$$4/3\text{trimer} \rightarrow \text{tetramer} \tag{9}$$

Table 8
Calculated free energies of THF solvated dimer formation (kcal/mol per Li)

Molecule	Temp (K)	6-31+G(d)	6-311+G(2df,2pd)
1	200	−0.796	−1.80
2	200	−2.70	−5.92
3	200	−6.53	−4.61
4	200	−2.23	−4.25
1	298.15	−1.98	−2.99
2	298.15	−3.79	−7.01
3	298.15	−7.90	−5.98
4	298.15	−3.80	−5.81

Table 9
Calculated free energies of THF solvated *anti*-trimer formation (kcal/mol per Li)

Molecule	Temp (K)	6-31+G(d)	6-311+G(2df,2pd)
1	200	−6.56	−3.17
2	200	−1.61	2.36
3	200	−2.02	3.19
4	200	−6.05	−1.04
1	298.15	−6.10	−2.70
2	298.15	−0.834	3.14
3	298.15	−1.03	4.16
4	298.15	−5.49	−0.489

Table 10
Calculated free energies of THF solvated *syn*-trimer formation (kcal/mol per Li)

Molecule	Temp (K)	6-31+G(d)	6-311+G(2df,2pd)
1	200	−4.04	−3.04
2	200	1.17	7.24
3	200	−2.10	1.20
4	200	−5.80	−1.38
1	298.15	−3.63	−2.63
2	298.15	1.83	7.91
3	298.15	−1.40	1.90
4	298.15	−5.16	−0.742

Table 11
Calculated free energies of THF solvated tetramer formation from the dimer (Eq. 13, kcal/mol per Li)

Molecule	Temp (K)	6-31+G(d)	6-311+G(2df,2pd)
1	200	−7.05	−0.0260
2	200	−4.48	2.54
3	200	−7.91	−0.552
4	200	−7.60	3.29
1	298.15	−5.77	1.25
2	298.15	−3.32	3.70
3	298.15	−6.72	0.643
4	298.15	−6.50	4.40

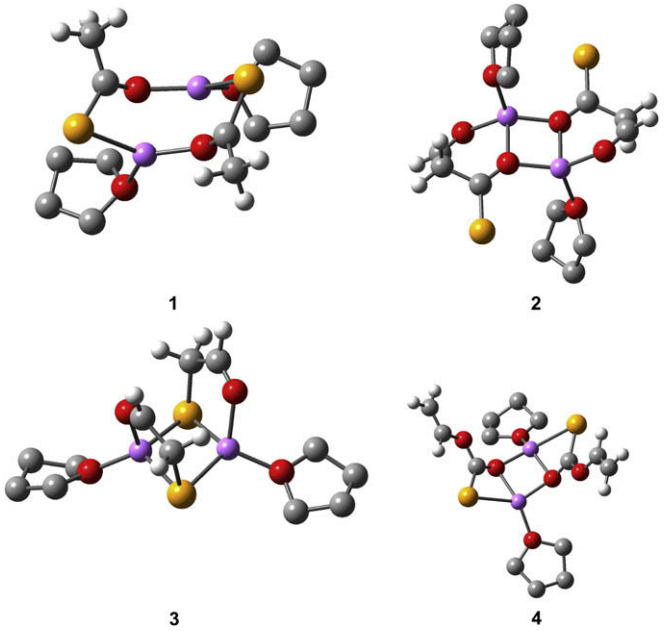

Figure 6. Optimized geometries of THF solvated dimers of compounds **1**–**4**.

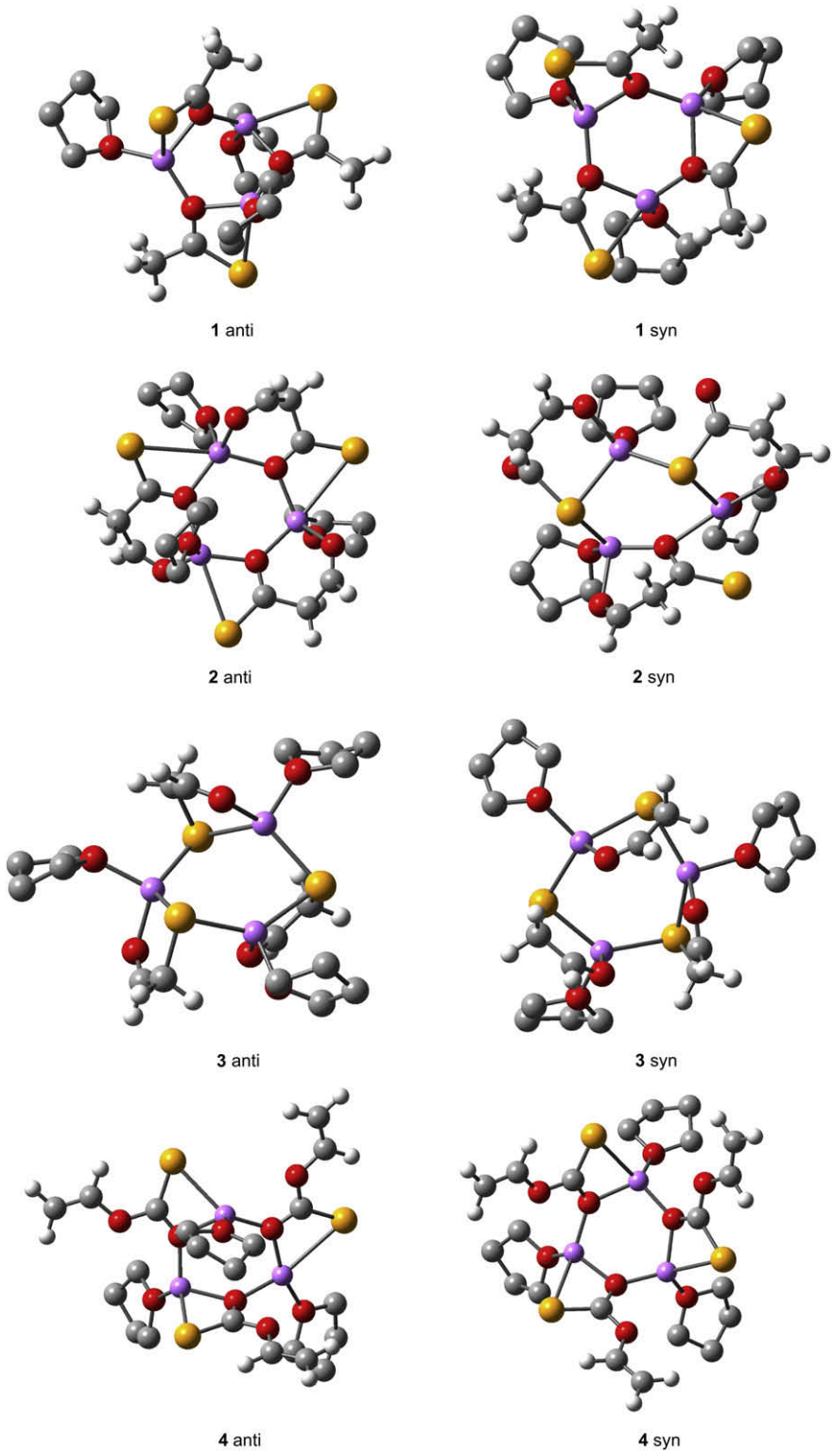

Figure 7. Optimized geometries of THF solvated trimers of compounds **1**–**4**.

In THF solution the monomers of compounds **1**–**4** could possibly exist either at the disolvate or trisolvates, and the third solvation energies were calculated according to Eq. 10, and listed in Table 7. In each case the third solvation energy was endergonic, and this energy was underestimated with the 6-31+G(d) basis set. Therefore, the disolvated form was used in subsequent calculations. As in the gas phase, solvated **5** optimized to a complex between **3** and CO. The optimized geometries of the disolvated monomers are shown in Figure 5.

$$\text{Monomer}\cdot 2\text{THF} + \text{THF} \rightarrow \text{Monomer}\cdot 3\text{THF} \qquad (10)$$

The free energies of solvated dimer, trimer, and tetramer formation were calculated according to Eqs. 11–13. The calculated free energies are listed in Tables 8–11, and the optimized geometries of

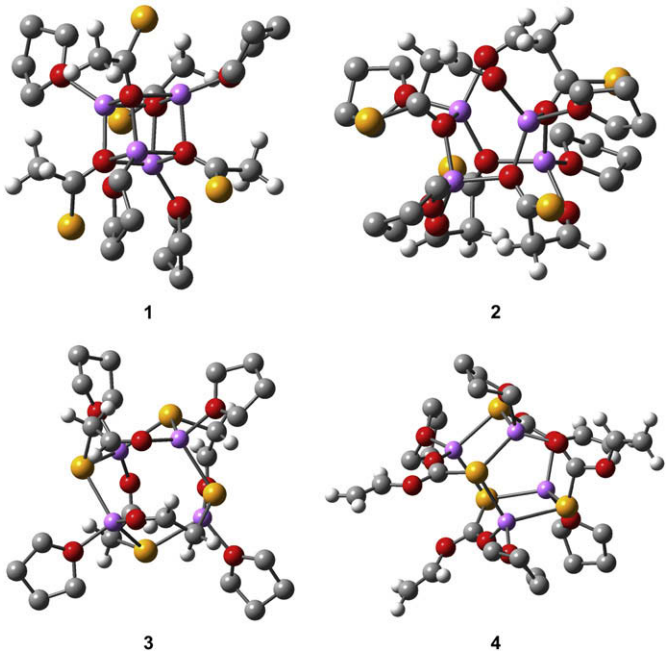

Figure 8. Optimized geometries of THF solvated tetramers of compounds **1**–**4**.

the aggregates are shown in Figures 6–9. In general, the aggregation free energies are less exergonic in THF solution than those in the gas phase. Comparison of Figures 1 and 5 shows that the intramolecular O–Li chelation that stabilized monomeric **2** in the gas phase is disrupted in solution. The same is true in the dimeric form, as seen from Figure 6. The result is that the dimerization free energy of **2** in solution is more in line with those of **1**, **3**, and **4**. Although the dimer and trimer of **5** optimized to local minima, they were high energy species relative to their isomer (**4**) and are not further considered.

$$2\text{monomer}\cdot 2\text{THF} \rightarrow \text{dimer}\cdot 2\text{THF} + 2\text{THF} \quad (11)$$

$$3/2\text{dimer}\cdot 2\text{THF} \rightarrow \text{trimer}\cdot 3\text{THF} \quad (12)$$

$$2\text{dimer}\cdot 2\text{THF} \rightarrow \text{tetramer}\cdot 4\text{THF} \quad (13)$$

In contrast to the gas phase, the most stable solvated trimers may be either in the *syn* or *anti* forms, as indicated by the data in Tables 9 and 10. The optimized trimer geometries are shown in Figure 7. The relative stability of the *anti* and *syn* forms appears to be a balance between steric effects and maximization of the lithium atom chelation. With compounds **1** and **2**, the *anti* form is favored by up to several kcal/mol, as that isomer appears to maximize the lithium coordination to both oxygen and selenium. The *syn* form of **3** is favored, and the two isomers of **4** are of comparable energy.

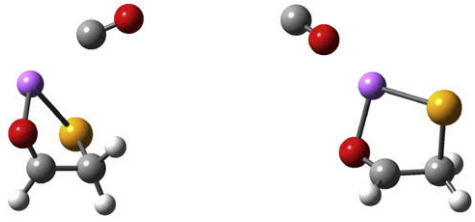

Figure 9. C-complex and O-complex forms of intermediate **5**.

Table 12
Calculated free energies of THF solvated tetramer formation from the most stable trimer (Eq. 14, kcal/mol per Li)

Molecule	Temp (K)	6-31+G(d)	6-311+G(2df,2pd)
1	200	−0.481	3.14
2	200	−2.86	0.184
3	200	−5.81	−1.75
4	200	−1.55	4.33
1	298.15	0.330	3.95
2	298.15	−2.48	0.566
3	298.15	−5.31	−1.26
4	298.15	−1.00	4.88

As was done for the gas-phase structures, the free energies of solvated tetramer formation were calculated via the dimer (Eq. 13) and via the trimer (Eq. 14). The data in Tables 11 and 12 show that for the most part, solvated tetramer formation is less favorable than trimer formation. This is apparently due to less chelation in the distorted tetramers. An exception is compound **3**, for which lithium chelation appears to be maximized in the tetramer. The optimized geometries are shown in Figure 8.

$$4/3\text{trimer}\cdot 3\text{THF} \rightarrow \text{tetramer}\cdot 4\text{THF} \quad (14)$$

Although intermediate **5** turned out to be a complex between **3** and CO, rather than the structure depicted in Scheme 1, it is likely to be a key intermediate in the CO insertion reaction. We therefore investigated two key reaction steps: the formation of **4** from **5**, and the elimination of SeCO from **5** to form the enolate–SeCO complex, which would lead to **4** by an alternate pathway. Since we have observed that the carbonylation reaction does not occur with the sulfur analog of **3**, we compared these reaction steps via both **5**–S and **5**–Se to better understand the role of selenium. A complete discussion of the role of aggregation and solvation in this reaction step is beyond the scope of this work, and will be published as a separate paper in the future. Nevertheless, examination of the gas-phase monomer provides valuable insight into the reaction mechanism. Preliminary results suggest that THF solvation results in qualitatively similar transition structures.

Closer examination of **5** showed that it can exist as either a C-bonded or O-bonded complex to the lithium atom, as shown in Figure 9. Similar structures were found for the sulfur analog of **5**. The C-bonded selenium complex reacted to form the enolate–SeCO complex, which is believed to further react forming **4**. This reaction is depicted in Figure 10. The sulfur analog reacted by a similar mechanism.

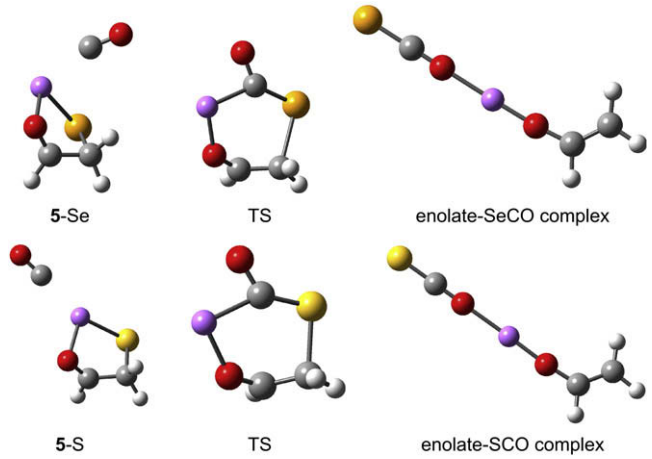

Figure 10. Reaction of **5**–Se (top) and **5**–S (bottom) to form enolate complexes with SeCO or SCO.

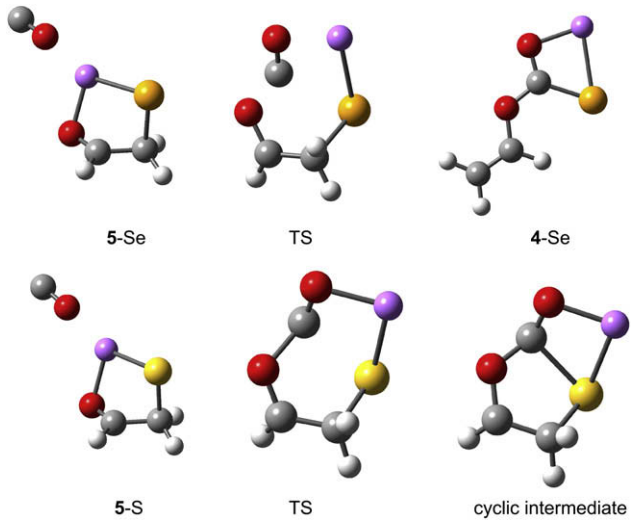

Figure 11. Reaction of **5**–Se (top) and **5**–S (bottom) to form **4**–Se and a cyclic sulfur-containing intermediate.

Table 13
MP2/6-31+G(d) calculated activation free energies ($\Delta G^{\ddagger}_{298}$) for reactions of **5**–Se and **5**–S (kcal/mol)

Reaction	**5**–Se	**5**–S
5→**4**	51.2	66.1
5→Li enolate–SeCO (SCO)	61.6	55.5

A single step rearrangement of **5**–Se to **4**–Se took place via the O-bonded complex, as shown in Figure 11. The analogous reaction of **5**–S was calculated to go by a similar pathway by the B3LYP method, but the MP2 calculations showed a similar transition structure that led to a cyclic species. This is consistent with the reported affinity of carbamoyllithium intermediates toward sulfur and sulfur-containing compounds.[44]

The data in Table 13 show the calculated barrier heights for the reactions of **5**–Se and **5**–S. For reasons that are still poorly understood, calculated absolute barrier heights of many organolithium reactions are quite high compared to the limited experimental data that are available. However, calculated relative barrier heights have generated results that were consistent with the experimental data for other organolithium systems.[45] Although inclusion of solvation and aggregation effects may lower these activation barriers somewhat, calculation of absolute barrier heights is likely to be much more complex, and may depend not only on solvation, but also on interaction with nearby ions and other organolithium species. In spite of those limitations, we see that the direct reaction of **5**–Se to **4**–Se is the favored reaction pathway. In the sulfur analog that pathway has a much higher activation barrier and it leads to a different product. The reaction of **5**–S is predicted to favor the indirect pathway via the enolate–SCO complex, but with an activation free energy higher than that of the direct reaction of **5**–Se. This is consistent with the observation that carbonylation of **3**–Se occurs, but **3**–S does not. The details of these and other steps of the reaction mechanism are currently being examined in more detail, including the effects of solvation and aggregate formation.

4. Conclusions

The lithium–selenium compounds in this work exist as dimers or higher aggregates in the gas phase and in THF solution, with higher aggregates being favored in the absence of solvation. The compounds used in this study were small model systems, and the actual synthetic reagents may be less prone to trimer and tetramer formation due to greater steric strain. The presumed intermediate (**5**) does not exist as such as a monomer, but rather as a dipole–dipole complex between **3** and CO. Although aggregates of **5** did optimize to local minima, they were high energy species and are not likely to be significant participants in these reactions. The mechanism of rearrangement of **5**→**4** has not yet been completely determined, but the lowest energy pathway appears to be a direct reaction rather than elimination of SeCO. The calculated activation energies of this key reaction step are consistent with the observed reaction of **3**–Se with CO, whereas **3**–S is unreactive.

Acknowledgements

This research used resources of the National Energy Research Scientific Computing Center, which is supported by the Office of Science of the U.S. Department of Energy under Contract No. DE-AC03-76SF00098. Support was also provided by a Fisk University Presidential Research Award.

Supplementary data

Tables of optimized geometries and energies of all aggregates and transition structures. Supplementary data associated with this article can be found in the online version, at doi:10.1016/j.tet.2008.11.087.

References and notes

1. Carbonylation of lithio derivatives of hydrocarbons, which have pK_a values ranging from 18 to 31.5: (a) Maeda, H.; Fujiwara, S.; Shin-ike, T.; Kambe, N.; Sonoda, N. *J. Am. Chem. Soc.* **1996**, *118*, 8160; (b) Maeda, H.; Fujiwara, S.; Nishiyama, A.; Shin-ike, T.; Kambe, N,; Sonoda, N. *Synlett* **1997**, 342.
2. Carbonylation of lithium enolates of ketones,[a] aldehydes,[a] amides,[b] and esters[b]: (a) Fujiwara, S.; Nishiyama, A.; Shin-ike, T.; Kambe, N.; Sonoda, N. *Org. Lett.* **2004**, *6*, 453; (b) Kambe, N.; Nishiyama, A.; Fujiwara, S.; Shin-ike, T.; Sonoda, N. *Phosphorus, Sulfur Silicon Relat. Elem.* **2005**, 1001.
3. N-Carbonylation of lithium azaenolates of amides, formamides, ureas, and carbamates: Fujiwara, S.; Okada, K.; Shikano, Y.; Shimizu, Y.; Shin-ike, T.; Terao, J.; Kambe, N.; Sonoda, N. *J. Org. Chem.* **2007**, *72*, 273.
4. For a recent review on selenol esters: Fujiwara, S.; Kambe, N. Thio-, Seleno-, and Telluro-Carboxylic Acid Esters. In *Topics in Current Chemistry 251: Chalcogen Carboxylic Acid Derivatives*; Kato, S., Ed.; Springer: Berlin, 2005; pp 87–141.
5. Imidoylation of lithio derivatives of hydrocarbons: Fujiwara, S.; Maeda, H.; Matsuya, T.; Shin-ike, T.; Kambe, N.; Sonoda, N. *J. Org. Chem.* **2000**, *65*, 5022.
6. The reaction of lithium enolates of ketones with Se in the presence of additives such as HMPA followed by trapping with alkyl halides resulted in formation of α-alkylselenoketones. The yields were very low without additives: (a) Liotta, D.; Zima, G.; Barnum, C.; Saindane, M. *Tetrahedron Lett.* **1980**, *21*, 3643; (b) Swiss, K.; Choi, W.-B.; Mohan, J.; Barum, C.; Saindane, M.; Zima, G.; Liotta, D. *Heteroat. Chem.* **1990**, *1*, 141.
7. Theoretical study on generation of SeCO: de Souza, W. F.; Kambe, N.; Sonoda, N. *Chem. Lett.* **1996**, 155.
8. We already examined the reaction of isoselenocyanate, having isoelectronic structure with SeCO, with organolithium compounds focusing on the siteselectivities. Phenyllithium attacked selenium exclusively whereas lithium enolate of a ketone reacted with SeCO at both its *C*- and *O*-nucleophilic centers attacking the central carbon of SeCO: Maeda, H.; Kambe, N.; Sonoda, N.; Fujiwara, S.; Shin-ike, T. *Tetrahedron* **1996**, *52*, 12165.
9. For carbophilic addition of organocopper reagents to SeCO: Fujiwara, S.; Asai, A.; Shin-ike, T.; Kambe, N.; Sonoda, N. *J. Org. Chem.* **1998**, *63*, 1724.
10. Lewis, H. L.; Brown, T. L. *J. Am. Chem. Soc.* **1970**, *92*, 4664.
11. Kimura, B. Y.; Brown, T. L. *J. Organomet. Chem.* **1971**, *26*, 57.
12. Pratt, L. M.; Nguyen, S. C.; Thanh, B. T. *J. Org. Chem.* **2008**, *73*, 6086 and references within.
13. Wang, D. Z.-R.; Kim, Y.-J.; Streitwieser, A. *J. Am. Chem. Soc.* **2000**, *122*, 10754.
14. Nichols, M. A.; Leposa, C. M.; Hunter, A. D.; Zeller, M. *J. Chem. Crystallogr.* **2007**, *37*, 825.
15. Williard, P. G.; Carpenter, G. B. *J. Am. Chem. Soc.* **1985**, *107*, 3345.
16. Williard, P. G.; Carpenter, G. B. *J. Am. Chem. Soc.* **1986**, *108*, 462.
17. McNeil, A. J.; Toombes, G. E. S.; Gruner, S. M.; Lobkovsky, E.; Collum, D. B.; Chandramouli, S. V.; Vanasse, B. J.; Ayers, T. A. *J. Am. Chem. Soc.* **2004**, *126*, 16559.
18. Amstutz, R.; Schweizer, W. B.; Seebach, D.; Dunitz, J. D. *Helv. Chim. Acta* **1981**, *64*, 2617.
19. Wen, J. Q.; Grutzner, J. B. *J. Org. Chem.* **1986**, *51*, 4220.
20. Jackman, L. M.; Szeverenyl, N. M. *J. Am. Chem. Soc.* **1977**, *99*, 4954.

21. Jackman, L. M.; Scarmoutzos, L. M.; DeBrosse, C. W. *J. Am. Chem. Soc.* **1987**, *109*, 5355.
22. Liou, L. R.; McNeil, A. J.; Ramirez, A.; Toombes, G. E. S.; Gruver, J. M.; Collum, D. B. *J. Am. Chem. Soc.* **2008**, *130*, 4859.
23. McKeever, L. D.; Waack, R.; Doran, M. A.; Baker, E. B. *J. Am. Chem. Soc.* **1969**, *91*, 1057.
24. Fraenkel, G.; Henrichs, M.; Hewitt, J. M.; Su, B. M.; Geckle, M. J. *J. Am. Chem. Soc.* **1980**, *102*, 3345.
25. Bauer, W.; Winchester, W. R.; Schleyer, P. v. R. *Organometallics* **1987**, *6*, 2371.
26. Pratt, L. M.; Truhlar, D. G.; Cramer, C. J.; Kass, S. R.; Thompson, J. D.; Xidos, J. D. *J. Org. Chem* **2007**, *72*, 2962.
27. Romesberg, F. E.; Gilchrist, J. H.; Harrison, A. T.; Fuller, D. J.; Collum, D. B. *J. Am. Chem. Soc.* **1991**, *113*, 5751.
28. Lucht, B. L.; Collum, D. B. *J. Am. Chem. Soc.* **1995**, *117*, 9863.
29. Remenar, J. F.; Lucht, B. L.; Collum, D. B. *J. Am. Chem. Soc.* **1997**, *119*, 5567.
30. Lucht, B. L.; Collum, D. B. *Acc. Chem. Res.* **1999**, *32*, 1035.
31. Renaud, P.; Fox, M. A. *J. Am. Chem. Soc.* **1988**, *110*, 5705.
32. Rutherford, J. L.; Collum, D. B. *J. Am. Chem. Soc.* **1999**, *121*, 10198.
33. Pratt, L. M. *THEOCHEM* **2007**, *811*, 191.
34. Pratt, L. M.; Kwon, O.; Ho, T. C.; Nguyen, N. V. *Tetrahedron* **2008**, *64*, 5314.
35. Pratt, L. M.; Tran, D. H. P.; Tran, P. T. T.; Nguyen, N. V. *Bull. Chem. Soc. Jpn.* **2007**, *80*, 1587.
36. Pratt, L. M.; Ramachandran, B. *J. Org. Chem.* **2005**, *70*, 7238.
37. Pratt, L. M.; Mogali, S.; Glinton, K. *J. Org. Chem.* **2003**, *68*, 6484.
38. Mogali, S.; Darville, K.; Pratt, L. M. *J. Org. Chem.* **2001**, *66*, 2368.
39. Arvidsson, P. I.; Davidsson, O. *Angew. Chem., Int. Ed.* **2000**, *39*, 1467.
40. Arvidsson, P. I.; Davidsson, O.; Hilmersson, G. *Tetrahedron: Asymmetry* **1999**, *10*, 527.
41. Frisch, M. J.; Trucks, G. W.; Schlegel, H. B.; Scuseria, G. E.; Robb, M. A.; Cheeseman, J. R.; Montgomery, J. A., Jr.; Vreven, T.; Kudin, K. N.; Burant, J. C.; Millam, J. M.; Iyengar, S. S.; Tomasi, J.; Barone, V.; Mennucci, B.; Cossi, M.; Scalmani, G.; Rega, N.; Petersson, G. A.; Nakatsuji, H.; Hada, M.; Ehara, M.; Toyota, K.; Fukuda, R.; Hasegawa, J.; Ishida, M.; Nakajima, T.; Honda, Y.; Kitao, O.; Nakai, H.; Klene, M.; Li, X.; Knox, J. E.; Hratchian, H. P.; Cross, J. B.; Adamo, C.; Jaramillo, J.; Gomperts, R.; Stratmann, R. E.; Yazyev, O.; Austin, A. J.; Cammi, R.; Pomelli, C.; Ochterski, J. W.; Ayala, P. Y.; Morokuma, K.; Voth, G. A.; Salvador, P.; Dannenberg, J. J.; Zakrzewski, V. G.; Dapprich, S.; Daniels, A. D.; Strain, M. C.; Farkas, O.; Malick, D. K.; Rabuck, A. D.; Raghavachari, K.; Foresman, J. B.; Ortiz, J. V.; Cui, Q.; Baboul, A. G.; Clifford, S.; Cioslowski, J.; Stefanov, B. B.; Liu, G.; Liashenko, A.; Piskortz, P.; Komaromi, I.; Martin, R. L.; Fox, D. J.; Keith, T.; Al-Laham, M. A.; Peng, C. Y.; Nanayakkara, A.; Challacombe, M.; Gill, P. M. W.; Johnson, B.; Chem, W.; Wong, M. W.; Gonzalez, C.; Pople, J. A. *Gaussian 03, Revision A.1*; Gaussian: Pittsburgh, PA, 2003.
42. Pratt, L. M.; Merry, S.; Nguyen, S. C.; Quan, P.; Thanh, B. T. *Tetrahedron* **2006**, *62*, 10821.
43. Govender, U. P.; Letcher, T. M.; Garg, S. K.; Ahluwalia, J. C. *J. Chem. Eng. Data* **1996**, *41*, 147.
44. Mizuno, T.; Nishiguchi, I.; Hirashima, T. *Tetrahedron* **1993**, *49*, 2403.
45. Pasumansky, L.; Collins, C. J.; Pratt, L. M.; Nguyen, N. V.; Ramachandran, B.; Singaram, B. *J. Org. Chem.* **2007**, *72*, 971.